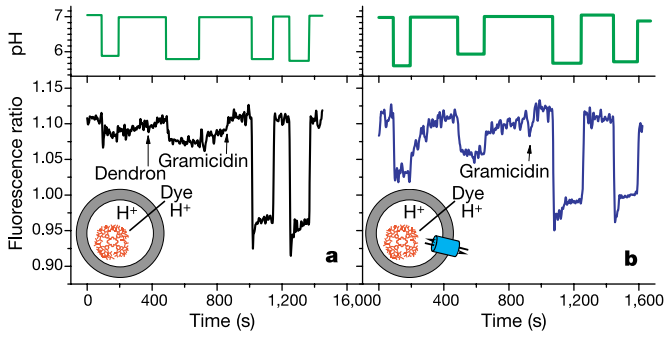

Figure 5 Proton transport through (4-3,4-3,5)12G2-CH_2-(Boc-L-Tyr-L-Ala-OMe) pores reconstituted in phospholipid liposomes (pH-jump experiments). **a**, Liposomes containing only the membrane-impermeable pH indicator[28] inside. **b**, Liposomes containing the pH indicator inside and the dendritic dipeptide pores. In both cases, arrows indicate the addition of the dendritic dipeptide or gramicidin as DMSO/THF solutions. pH jumps at 20 °C outside the liposome (induced by adding aliquots, about 10 μl, of HCl or KOH) were recorded by pH microelectrodes (upper graphs). pH jumps inside liposomes were assessed by fluorescence (I_{647}/I_{670}) (lower graphs). The signal of the total amount of captured pH dye was estimated by adding an excess of gramicidine. Liposomes were prepared by sonicating a 1/14 mass ratio of dendritic dipeptide in the presence of L-α-phosphatidylcholine (P5638 from Sigma) and a fluorescent membrane-impermeable pH indicator (G4 polyglutamic porphyrin-dendrimer)[28] in a phosphate buffer (10 mM K_2HPO_4, 50 mM KCl, pH = 7.0). The control experiment (**a**) has no dendron. Liposomes were purified from untrapped indicator by gel filtration on Sephadex (G200) and on anion exchange resin QAE Sepharose A50 and placed in a fluorimetric cell equipped with a stirrer. As expected from its hydrophobicity (un-optimized experiment **a**), the dendritic dipeptide was not delivered very effectively to liposomes by simply adding its solution in DMSO/THF: the addition increases permeability only slightly. In contrast, liposomes made of a lipid dendritic dipeptide mixture[27] (14/1 mass ratio lipid to dendron equivalent to an average of one to two pores per vesicle; Supplementary Section S10) yields permeable vesicles significantly more responsive to pH changes (**b**). Addition of gramicidin increases the magnitude of the jumps, suggesting that a small fraction of vesicles did not contain dendritic channels. Addition of 10 μl of DMSO alone does not affect permeability.

CH_2-[Boc-L-Tyr-L-Ala-OMe] was reconstituted[27] in the thermotropic bilayer lamellar phase and in liposomes produced from phospholipids (Supplementary Section S9). By monitoring the emission intensity of a pH-sensitive fluorescent dye[28] captured inside the liposomes, proton translocation mediated by dendritic pores and gramicidin channels can be evaluated (Fig. 5 and Supplementary Fig. SF19)[28,29]. Proton permeability of liposomes containing an average of one to two reconstituted dendritic pores (14/1 mass ratio phospholipid to dendritic dipeptide) was comparable in efficiency to those containing gramicidin channels. These results illustrate that supramolecular dendrimer chemistry[30] allows the controlled design of a range of periodic non-biological porous structures forming in solution and as films. □

Received 11 February; accepted 16 June 2004; doi:10.1038/nature02770.

1. Klug, A. From macromolecules to biological assemblies. *Angew. Chem. Int. Edn Engl.* **22,** 565–582 (1983).
2. Doyle, D. A. *et al.* The structure of the potassium channel: molecular basis of K^+ conduction and selectivity. *Science* **280,** 69–77 (1998).
3. Murata, K. *et al.* Structural determinants of water permeation through aquaporin-1. *Nature* **407,** 599–605 (2000).
4. van den Berg, B. *et al.* X-ray structure of a protein conducting channel. *Nature* **427,** 36–44 (2004).
5. Fernandez-Lopez, S. *et al.* Antibacterial agents based on the cyclic D,L-α-peptide architecture. *Nature* **412,** 452–455 (2001).
6. Ishii, D. *et al.* Chaperonin-mediated stabilization and ATP-triggered release of semiconductor nanoparticles. *Nature* **423,** 628–632 (2003).
7. Bayley, H. & Cremer, P. S. Stochastic sensors inspired by biology. *Nature* **413,** 226–230 (2001).
8. Ghadiri, M. R., Granja, J. R., Millligan, R. A., McRee, D. E. & Khazanovich, N. Self-assembling organic nanotubes based on a cyclic peptide architecture. *Nature* **366,** 324–327 (1993).
9. Schmitt, J.-L., Stadler, A.-M., Kyritsakas, N. & Lehn, J.-M. Helicity encoded molecular strands: efficient access by the hydrazone route and structural features. *Helv. Chim. Acta* **86,** 1598–1624 (2003).
10. Lehn, J.-M. *Supramolecular Chemistry. Concepts and Perspectives* 118 (VCH, Weinheim, 1995).
11. Bong, D. T., Clark, T. D., Granja, J. R. & Ghadiri, M. R. Self-assembling organic nanotubes. *Angew. Chem. Int. Edn Engl.* **40,** 989–1011 (2001).
12. Hill, D. J., Mio, M. J., Prince, R. B., Hughes, T. S. & Moore, J. S. A field guide to foldamers. *Chem. Rev.* **101,** 3893–4011 (2001).
13. Sakai, N. & Matile, S. Synthetic multifunctional pores: lessons from rigid-rod β-barrels. *Chem. Commun.*, 2514–2523 (2003).
14. Percec, V. *et al.* Controlling polymer shape through the self-assembly of dendritic side-groups. *Nature* **391,** 161–164 (1998).
15. Percec, V. *et al.* Self-organization of supramolecular helical dendrimers into complex electronic materials. *Nature* **419,** 384–387 (2002).
16. Percec, V., Cho, W.-D., Ungar, G. & Yeardley, D. J. P. Synthesis and NaOTf mediated self-assembly of monodendritic crown-ethers. *Chem. Eur. J.* **8,** 2011–2025 (2002).
17. Hudson, S. D. *et al.* Direct visualization of individual cylindrical and spherical dendrimers. *Science* **278,** 449–452 (1997).
18. Percec, V., Cho, W.-D., Ungar, G. & Yeardley, D. J. P. Synthesis and structural analysis of two constitutional isomeric libraries of AB_2-based monodendrons and supramolecular dendrimers. *J. Am. Chem. Soc.* **123,** 1302–1315 (2001).
19. Nelson, J. C., Saven, J. G., Moore, J. S. & Wolynes, P. G. Solvophobically driven folding of nonbiological oligomers. *Science* **277,** 1793–1796 (1997).
20. Brunsveld, L., Zhang, H., Glasbeek, M., Vekemans, J. A. J. M. & Meijer, E. W. Hierarchical growth of chiral self-assembled structures in protic media. *J. Am. Chem. Soc.* **122,** 6175–6182 (2000).
21. Chan, H. S., Bromberg, S. & Dill, K. A. Models of cooperativity in protein folding. *Phil. Trans. R. Soc. Lond. B* **348,** 61–70 (1995).
22. Engelkamp, H., Middelbeek, S. & Nolte, R. J. M. Self-assembly of disk-shaped molecules to coiled-coil aggregates with tunable helicity. *Science* **284,** 785–788 (2001).
23. Hirschberg, J. H. K. K. *et al.* Helical self-assembled polymers from cooperative stacking of hydrogen-bonded pairs. *Nature* **407,** 167–170 (2000).
24. Balagurusamy, V. S. K., Ungar, G., Percec, V. & Johansson, G. Rational design of the first spherical supramolecular dendrimers self-organized in a novel thermotropic cubic liquid-crystalline phase and the determination of their shape by X-ray analysis. *J. Am. Chem. Soc.* **119,** 1539–1555 (1997).
25. Hummer, G., Rasaiah, J. C. & Noworita, J. P. Water conduction through the hydrophobic channel of a carbon nanotube. *Nature* **414,** 188–190 (2001).
26. Cornelissen, J. J. L. M. *et al.* β-Helical polymers from isocyanopeptides. *Science* **293,** 676–680 (2001).
27. Rigaud, J.-L., Pitard, B. & Levy, D. Reconstitution of membrane proteins into liposomes: application to energy-transducing membrane proteins. *Biochim. Biophys. Acta* **1231,** 223–246 (1995).
28. Finikova, O. *et al.* Porphyrin and tetrabenzoporphyrin dendrimers: tunable membrane-impermeable fluorescent pH nanosensors. *J. Am. Chem. Soc.* **125,** 4882–4893 (2003).
29. Ghadiri, M. R., Granja, J. R. & Buehler, L. K. Artificial transmembrane ion channels from self-assembling peptide nanotubes. *Nature* **369,** 301–304 (1994).
30. Emrick, T. & Fréchet, J. M. J. Self-assembly of dendritic structures. *Curr. Opin. Colloid Interface Sci* **4,** 15–23 (1999).

Supplementary Information accompanies the paper on **www.nature.com/nature**.

Acknowledgements Financial support by the National Science Foundation, the Office of Naval Research and the P. Roy Vagelos Chair at the University of Pennsylvania is acknowledged. J.S. thanks the Isabel and Alfred Bader Foundation for a graduate fellowship, and U.E. acknowledges a Hans Werthén scholarship for postdoctoral studies. We also thank S.Z.D. Cheng for density measurements, and G. Ungar for reading the draft manuscript and for suggestions.

Competing interests statement The authors declare that they have no competing financial interests.

Correspondence and requests for materials should be addressed to V.P. (percec@sas.upenn.edu).

Quantification of modelling uncertainties in a large ensemble of climate change simulations

James M. Murphy[1], David M. H. Sexton[1], David N. Barnett[1], Gareth S. Jones[1], Mark J. Webb[1], Matthew Collins[1] & David A. Stainforth[2]

[1]*Hadley Centre for Climate Prediction and Research, Met Office, FitzRoy Road, Exeter EX1 3PB, UK*
[2]*Department of Physics, University of Oxford, Parks Road, Oxford OX1 3PU, UK*

Comprehensive global climate models[1] are the only tools that account for the complex set of processes which will determine future climate change at both a global and regional level. Planners are typically faced with a wide range of predicted changes from different models of unknown relative quality[2,3], owing to large but unquantified uncertainties in the modelling

process[4]. Here we report a systematic attempt to determine the range of climate changes consistent with these uncertainties, based on a 53-member ensemble of model versions constructed by varying model parameters. We estimate a probability density function for the sensitivity of climate to a doubling of atmospheric carbon dioxide levels, and obtain a 5–95 per cent probability range of 2.4–5.4 °C. Our probability density function is constrained by objective estimates of the relative reliability of different model versions, the choice of model parameters that are varied and their uncertainty ranges, specified on the basis of expert advice. Our ensemble produces a range of regional changes much wider than indicated by traditional methods based on scaling the response patterns of an individual simulation[5,6].

Detailed and multi-variable predictions of anthropogenic climate change are required for impact assessments[6]. Only comprehensive three-dimensional global climate models[1] (GCMs) are capable of providing such information. By simulating the key physical processes involved, they can represent the complex nonlinear interactions that influence climate change at a regional level, including changes in the frequency of damaging storms and other extreme events[7]. Yet GCM predictions are currently subject to considerable uncertainties in the modelling process[4,8], to the extent that different models often disagree even on the sign of the changes expected in particular regions[2]. It is therefore essential that GCM predictions are accompanied by quantitative estimates of the associated uncertainty in order to render them usable in planning mitigation and adaptation strategies[6].

Modelling uncertainties arise from fundamental choices made when building the GCM (for example, grid resolution), and from the parameterization of processes unresolved at the grid scale (for example, cloud formation). Here we provide a systematic investigation of modelling uncertainty by varying the settings of GCM parameters whose values cannot be accurately determined from observations[9]. The range of predictions obtained should be recognized as a lower limit, which could increase once the approach is generalized to sample structural modelling uncertainties[10] arising from choices such as resolution, the set of processes included in the model and the basic assumptions on which its parameterizations are based[11].

We focus on uncertainties in the equilibrium response to a doubling of atmospheric CO_2 assuming no changes in other external forcing agents. Our GCM consists of the atmospheric model HadAM3[12] coupled to a mixed layer ocean that allows integration to equilibrium in a few decades. This enables us to increase ensemble size at the expense of neglecting ocean circulation feedbacks. There are of the order of 100 parameters in HadAM3, consisting of logical switches or variable coefficients or thresholds. A subset of 29 parameters was identified by modelling experts as controlling key physical characteristics of sub-grid scale atmospheric and surface processes. We perturbed these one at a time relative to the standard version of the GCM[12] (hereafter STD), creating a perturbed physics ensemble (PPE) of 53 model versions each used to simulate present-day and doubled CO_2 climates.

Uncertainty in regional climate change is commonly estimated by scaling a pattern of change from a single GCM simulation according to a range of possible changes in globally averaged surface temperature[6]. We assess this approach by synthesizing an ensemble of response patterns, in which the pattern of STD is scaled using 52 ratios of the climate sensitivity of each PPE member relative to STD. The ensemble standard deviations of synthesized and simulated responses are then compared (the black and red curves in Fig. 1). Scaling the pattern of a single ensemble member fails to reproduce the range of simulated regional changes, particularly for variables other than surface temperature (we show changes in precipitation and sea level pressure). For example, the scaling approach captures less than 10% of the variance of tropical precipitation changes. This has fundamental implications for the way in which climate predictions are produced. A single prediction of future climate made with even the most sophisticated GCM will be of limited use for impact assessments. Only large ensembles of GCM predictions sampling the widest possible range of modelling uncertainties can provide a reliable specification of the spread of possible regional changes.

The spread of changes obtained from the PPE is influenced by both process uncertainties and internal variability arising from random climate variations[13]. We find that the spread in surface warming predictions is dominated by process uncertainties (compare red and blue curves in Fig. 1). For precipitation and sea level pressure, internal variability makes a much larger contribution, particularly in extratropical regions. Narrowing the uncertainties arising from internal variability will require ensembles of simulations started from different initial conditions, while the minimization of process uncertainties will require the development of more accurate parameterizations for use in GCMs.

The PPE also allows us to obtain credible quantitative estimates of the robustness of the simulated changes to the modelling uncertainties explored (Fig. 2). Robustness is high almost everywhere for surface temperature, but varies widely with location for precipitation and sea level pressure. The type of information shown in Figs 1 and 2 provides a basis for constructing climate scenarios in which the signal of expected regional change can be reliably

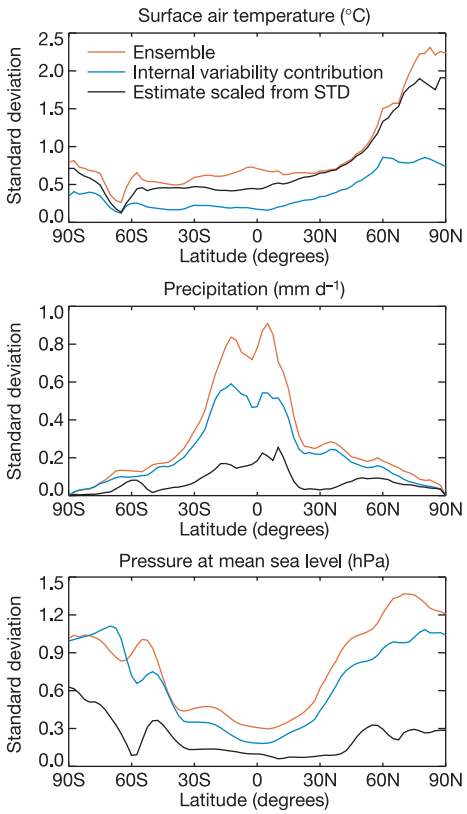

Figure 1 Zonal means of the ensemble standard deviation at individual 300 × 300 km^2 model grid boxes of the equilibrium response to doubled CO_2. Values are shown for 20 yr averages of December to February climate for surface air temperature, precipitation and pressure at mean sea level. The red curve shows results from the perturbed physics ensemble (PPE), the spread in which arises from both process uncertainties and internal variability. The blue curve shows the spread arising from internal variability alone, estimated by running 600 yr present-day and doubled CO_2 integrations of STD (the standard model version) and calculating the standard deviation of the response from constituent 20 yr periods. The black curve shows an attempt to reproduce the red curve by scaling the response patterns of STD according to the global climate sensitivities of the other 52 members of the PPE as described in the text.

separated from the noise of natural variability, thus providing planners with an improved basis for the development of appropriate response strategies[6]. We emphasize that the spread of regional changes estimated from our PPE, while substantially larger than would have been inferred by scaling the patterns of one of its members (see above), is likely to increase once it becomes possible to sample modelling uncertainties more comprehensively.

An important benchmark of anthropogenic climate change is the climate sensitivity, defined as the equilibrium response of globally averaged annual surface temperature to doubled CO_2. We estimate probability density functions (PDFs) for climate sensitivity from the 53-member PPE by assuming that the impacts of individual parameter perturbations, both on simulated present-day climate and the feedbacks that determine sensitivity, combine linearly. This allows us to predict the results of a much larger ensemble containing 4×10^6 model versions with randomly chosen multiple parameter perturbations generated by assuming a uniform distribution for each parameter within the range of values estimated by experts (see Methods). The blue curve in Fig. 3 shows a PDF obtained by assuming all 4×10^6 predictions of sensitivity to be equally reliable. It gives a median value of 2.9 °C with a spread (corresponding to a 5–95% probability range) of 1.9–5.3 °C.

The assumption of equal reliability between members of the GCM ensemble is standard in climate prediction[4,14], yet represents a major difficulty since variations in quality between models are ignored. Here we introduce a Climate Prediction Index (CPI), an objective measure of reliability that can be used to weight different GCMs according to the estimated relative likelihood that they will correctly predict climate change in the real world[15]. Reliability can potentially be quantified by verifying simulations of climate change during the past century[10,16], or of a stationary climate assumed to correspond to some recent period[17,18]. Our experimental design precludes the former approach, so we base the CPI on a broad range of present-day climate variables (Fig. 4 and Supplementary Information). Most PPE members occupy a rather narrow range of overall CPI values, though the range is much wider for some of its components, notably those associated with cloud, radiation and moisture. We justify use of the CPI to weight climate change predictions from a 'perfect model' test in which pairs of PPE members are compared against each other, one member taken to represent the observed climate system and the other a model simulation of it. For each possible pair, we calculated a CPI score and the magnitude of the difference between the simulated and 'observed' climate sensitivity. Amongst poor predictions of the 'observed' response (differences in sensitivity above the median) the CPI score was 2.7 times more likely to be poor (that is, above its median value) than good, and vice versa for good predictions of the response (sensitivity differences below the median).

We produce a likelihood-weighted PDF of climate sensitivity (the red curve in Fig. 3) by estimating the CPI of the 4×10^6 model versions used to produce the blue curve, and weighting their predictions of sensitivity according to $\exp(-0.5\mathrm{CPI}^2)$ (see Methods). This results in a narrowing of the 5–95% probability range to 2.4–5.4 °C, while the median value increases to 3.5 °C. Previously, PDFs of climate sensitivity have been obtained by exploring the range of predictions of simpler climate models[19–21] consistent with uncertainties in observed transient climate change and forcing[22,23]. Our PDFs are (to our knowledge) the first to be determined by systematically exploring uncertainties in the complex variety of processes that actually determine climate sensitivity. They indicate a smaller probability for sensitivities of 2 °C or less than is implied by studies comparing observed historical changes with simulations by simple models[21] or GCMs[24]. Our PDFs are contingent upon the structural choices made in building our GCM, the use of a linear prediction scheme, the choice and application of observational constraints and the choice of parameters for perturbation. They also depend on the assumed distributions of parameter values, although we found that increasing their expert-specified ranges had only a modest impact on the 5–95% probability range

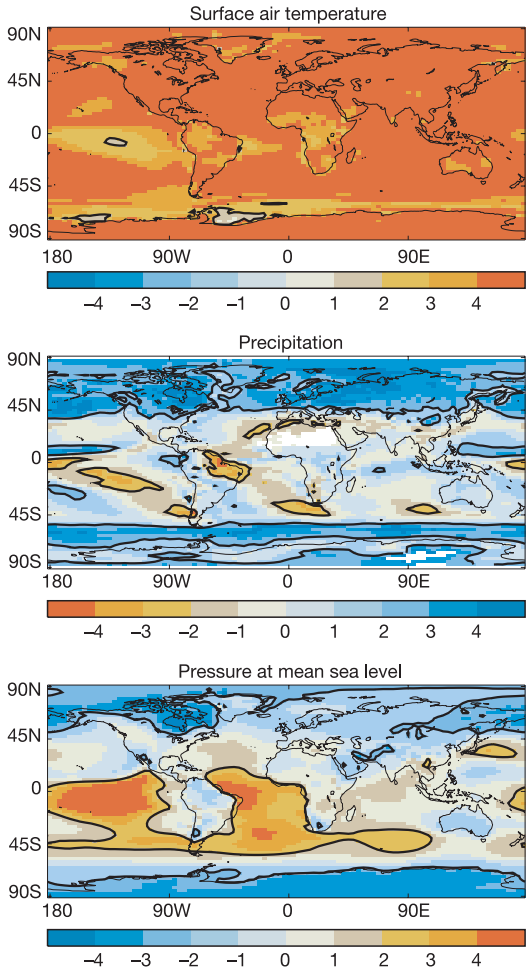

Figure 2 Robustness of simulated changes in surface air temperature, precipitation and pressure at mean sea level in response to doubled CO_2. The maps show changes in 20 yr means of December to February climate, averaged over the PPE of GCM versions and divided by the ensemble standard deviation of the changes. Values outside the range ±2 (highlighted by the black contour) are taken to indicate a robust response.

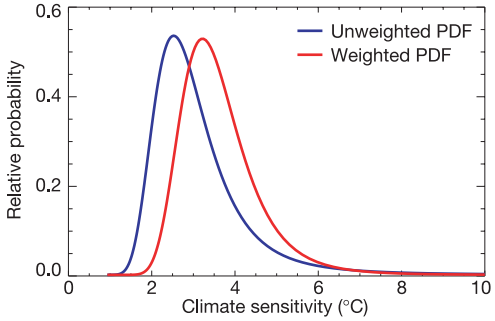

Figure 3 Probability distributions of climate sensitivity. These were obtained using linear statistical estimation of GCM predictions likely to result from a large PPE designed to sample the model parameter space comprehensively, with (red) and without (blue) weighting according to the estimated reliability of model versions based on the Climate Prediction Index (CPI). Details in text.

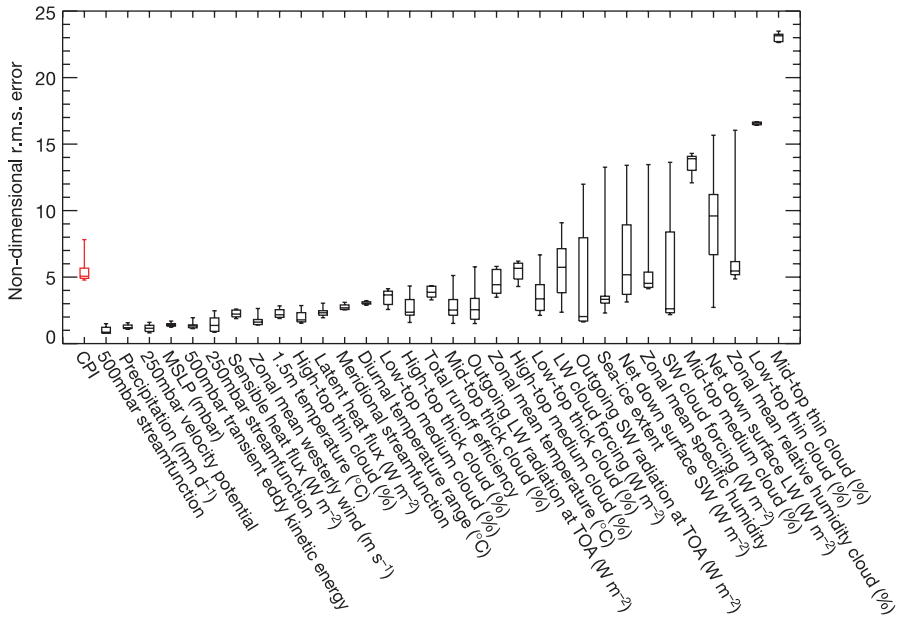

Figure 4 Values of the Climate Prediction Index (CPI) (red box and bars) and its components (black boxes and bars) from the PPE. The 32 components represent surface and atmospheric variables, and are calculated as the r.m.s. difference between simulated and observed present-day climatological mean patterns divided by the r.m.s value of the standard deviation of simulated interannual variations. The plot shows averages of values calculated separately for each season of the year. Bars show the full range of the ensemble distribution of values, boxes show the range encompassed by the 5th and 95th percentiles, and the horizontal line within each box shows the median. The CPI is calculated as the r.m.s. value of the 32 components for a given ensemble member. All components are weighted equally, apart from the nine fields of cloud cover which receive a relative weight of 1/3 since observations of high, medium and low cloud are interdependent for a given thickness category. LW, longwave; SW, shortwave; TOA, top of atmosphere; MSLP, mean sea level pressure.

associated with our CPI-weighted PDF (Supplementary Information). Our experimental design does not sample ocean circulation feedbacks or the impact of biases in the present-day simulations of sea surface temperature (SST). However these are likely to exert only a modest influence on global climate sensitivity (refs 25–28 and Supplementary Information). The impact of neglecting structural modelling uncertainties cannot yet be quantified, however the range obtained from our unweighted PDF encompasses the range of climate sensitivities (2.0–5.1 °C) found in an ensemble of 15 GCMs developed at different modelling centres and containing structural variations[4].

The PPE approach will be further developed to produce PDFs of time-dependent regional changes for use in assessments of climate-related risks[6]. This will require ensemble simulations of twentieth and twenty-first century climate using versions of HadAM3 coupled to a comprehensive ocean component[1], allowing us to account for the effects of oceanic thermal inertia, circulation changes and process uncertainties. These ensembles will need to sample multiple parameter perturbations, since our assumption that individual perturbations combine linearly is unlikely to be valid at a regional scale[29]. Ensemble size will be increased by including results from simulations run on personal computers owned by members of the public and businesses (see refs 29, 30, and ⟨http://www.climateprediction.net⟩). We also encourage other climate modelling institutes to perform similar ensemble experiments with their GCMs. These could then be combined with ours to create 'super-ensembles' that sample structural uncertainties. □

Methods

GCM integrations and parameter perturbations

For each ensemble member, control (that is, present day) and doubled CO_2 GCM integrations were run to equilibrium followed by a further 20 yr from which climate statistics were generated. The GCM used a mixed layer ocean with prescribed heat transports, which ensured that time averaged SSTs remained close to observed climatological values in the control simulations. However SSTs were allowed to vary freely in response to natural and forced variations. The selection of parameter perturbations was designed to sample uncertainties in a wide range of processes without making a priori assumptions about the relative importance of different climate change feedbacks[8]. The perturbations affected large-scale cloud and precipitation, convection, radiation, dynamics, boundary layer transports, land surface processes and sea ice. Parameters were perturbed either by changing a logical switch or by setting a coefficient or threshold to a minimum, intermediate or maximum value specified by experts, one of these (often, but not always, the intermediate value) being that used in STD. See Supplementary Information for details.

Weighting the predictions of ensemble members

We seek to weight model predictions of climate sensitivity according to the likelihood that the simulation of present-day climate is consistent with observations. The probability that a simulated variable m belongs to a population of observations of mean o and standard deviation σ is proportional to $\exp\{-0.5\ (m-o)^2/\sigma^2\}$, assuming gaussian statistics. In principle, the likelihood of the model can be obtained by calculating the joint probability of all model variables, taking into account their covariances and allowing for errors in the verifying observations. In practice, the required error statistics were not available, because our model versions were not run long enough to estimate their covariance matrices and observational errors are not known for most of the variables included in the CPI. We therefore make simplifying assumptions in order to obtain a likelihood-based weight. Our choice is $\exp(-0.5\mathrm{CPI}^2)$, which represents an estimate of likelihood obtained by normalizing the error variance in simulated climate by the variance of simulated interannual variations and then averaging the normalized error variance over a wide range of climate variables. Our decision to weight each component equally when forming the CPI represents an a priori assumption that changes in climate sensitivity are equally affected by all model variables.

Production of probability distributions for climate sensitivity

We obtained statistical predictions of CPI and climate sensitivity for 4×10^6 random combinations of multiple parameter perturbations generated by assuming a uniform prior for each parameter within the range specified by experts. Predictions of climate sensitivity (ΔT) were made in terms of the feedback strength λ, defined as $\lambda = \Delta Q/\Delta T$, ΔQ being the radiative forcing due to doubling CO_2. We predicted values of CPI and λ by assuming that the effects of individual parameter perturbations on present-day climate fields and feedback strength can be interpolated linearly between the values sampled in our PPE, and that the effects of individual parameter perturbations combine linearly and independently.

The predictions of λ are sensitive to λ_{std}, the feedback strength found in STD, since all perturbations are calculated relative to this value. We therefore repeated the calculation for 21 values of λ_{std} sampling at equal intervals the $\pm$ two standard deviation uncertainty range of 600 yr mean values (1.069–1.088 $\mathrm{W\,m^{-2}\,K^{-1}}$) estimated from 600 yr control and $2 \times CO_2$ integrations of STD. For each of these $21 \times 4 \times 10^6$ predictions, we calculated an

associated error as the sum of terms arising from nonlinear interactions between parameter perturbations and noise (natural variability) in the model simulations used to construct the predictions. Both error terms were assumed to be independent of location in parameter space (and hence climate sensitivity). The first term was estimated by verifying our statistical predictions against simulations made with 13 model versions containing multiple parameter perturbations and simulating climate sensitivities in the range 3.1–4.9 °C. The second term was estimated from the long STD experiment (See Supplementary Information). Each of our $21 \times 4 \times 10^6$ predictions of λ was then expressed as a gaussian distribution accounting for its expected error. A PDF of feedback strength was derived by combining the resulting $21 \times 4 \times 10^6$ distributions, each weighted according to the probability of the relevant value of λ_{std}.This was converted into a PDF of climate sensitivity using $\Delta T = \Delta Q/\lambda$, giving the blue PDF in Fig. 3. The red PDF was derived in the same manner, except that a further weighting of $\exp(-0.5\mathrm{CPI}^2)$ was applied to each of the gaussian distributions of λ. Results from our 13 verifying multiple perturbation experiments showed that our statistical predictions of CPI were close to the simulated values and that the predictions of λ carried a standard error of about $0.15\,\mathrm{W\,m^{-2}\,K^{-1}}$, arising mainly from the nonlinear effects of combining parameter perturbations[29].

Received 29 March; accepted 16 June 2004; doi:10.1038/nature02771.

1. Gordon, C. *et al.* The simulation of SST, sea ice extents and ocean heat transports in a version of the Hadley Centre coupled model without flux adjustments. *Clim. Dyn.* **16,** 147–168 (2000).
2. Giorgi, F. & Francisco, R. Evaluating uncertainties in the prediction of regional climate change. *Geophys. Res. Lett.* **27,** 1295–1298 (2000).
3. Allen, M. R. & Ingram, W. J. Constraints on future changes in climate and the hydrological cycle. *Nature* **419,** 224–232 (2002).
4. Cubasch, U. *et al.* in *Climate Change 2001, The Science of Climate Change* Ch. 9 (eds Houghton, J. T. *et al.*) 527–582 (Cambridge Univ. Press, Cambridge, 2001).
5. Allen, M. R., Stott, P. A., Mitchell, J. F. B., Schnur, R. & Delworth, T. L. Quantifying the uncertainty in forecasts of anthropogenic climate change. *Nature* **417,** 617–620 (2000).
6. Mearns, L. O. *et al.* in *Climate Change 2001, The Science of Climate Change* Ch. 13 (eds Houghton, J. T. *et al.*) 739–768 (Cambridge Univ. Press, Cambridge, 2001).
7. Meehl, G. A. *et al.* Trends in extreme weather and climate events: issues related to modelling extremes in projections of future climate change. *Bull. Am. Meteorol. Soc.* **81,** 427–436 (2000).
8. Stocker, T. F. *et al.* in *Climate Change 2001, The Science of Climate Change* Ch. 7 (eds Houghton, J. T. *et al.*) 417–470 (Cambridge Univ. Press, Cambridge, 2001).
9. Randall, D. A. & Wielicki, B. A. Measurements, models and hypotheses in the atmospheric sciences. *Bull. Am. Meteorol. Soc.* **78,** 399–406 (1997).
10. Wigley, T. M. L. & Raper, S. C. B. Interpretation of high projections for global-mean warming. *Science* **293,** 451–454 (2001).
11. Palmer, T. N. A nonlinear dynamical perspective on model error: A proposal for non-local stochastic-dynamic parametrization in weather and climate prediction models. *Q.J.R. Meteorol. Soc.* **127,** 279–303 (2001).
12. Pope, V. D., Gallani, M., Rowntree, P. R. & Stratton, R. A. The impact of new physical parameterisations in the Hadley Centre climate model—HadAM3. *Clim. Dyn.* **16,** 123–146 (2000).
13. Keen, A. B. & Murphy, J. M. Influence of natural variability and the cold start problem on the simulated transient response to increasing CO_2. *Clim. Dyn.* **13,** 847–864 (1997).
14. Palmer, T. N. & Räisänen, J. Quantifying the risk of extreme seasonal precipitation events in a changing climate. *Nature* **415,** 514–517 (2002).
15. Leroy, S. S. Detecting climate signals: Some Bayesian aspects. *J. Clim.* **11,** 640–651 (1998).
16. Stott, P. A. & Kettleborough, J. A. Origins and estimates of uncertainty in predictions of twenty-first century temperature rise. *Nature* **416,** 723–726 (2002).
17. Giorgi, F. & Mearns, L. O. Calculation of average, uncertainty range, and reliability of regional climate changes from AOGCM simulations via the "Reliability Ensemble Averaging" (REA) method. *J. Clim.* **15,** 1141–1158 (2002).
18. Giorgi, F. & Mearns, L. O. Probability of regional climate change based on the Reliability Ensemble Averaging (REA) method. *Geophys. Res. Lett.* **30,** 1629 (2003).
19. Andronova, N. G. & Schlesinger, M. E. Objective estimation of the probability density function for climate sensitivity. *J. Geophys. Res.* **106,** 22605–22612 (2001).
20. Forest, C. E., Stone, P. H., Sokolov, A. P., Allen, M. R. & Webster, M. D. Quantifying uncertainties in climate system properties with the use of recent climate observations. *Science* **295,** 113–117 (2002).
21. Knutti, R., Stocker, T. F., Joos, F. & Plattner, G. K. Constraints on radiative forcing and future climate change from observations and climate model ensembles. *Nature* **416,** 719–723 (2002).
22. Gregory, J. M., Stouffer, R. J., Raper, S. C. B., Stott, P. A. & Rayner, N. A. An observationally based estimate of the climate sensitivity. *J. Clim.* **15,** 3117–3121 (2002).
23. Anderson, T. L. *et al.* Climate forcing by aerosols—a hazy picture. *Science* **300,** 110–111 (2003).
24. Barnett, T. P., Pierce, D. W. & Schnur, R. Detection of anthropogenic climate change in the world's oceans. *Science* **292,** 270–274 (2001).
25. Boer, G. J. & Yu, B. Dynamical aspects of climate sensitivity. *Geophys. Res. Lett.* **30,** 1135 (2003).
26. Stouffer, R. J. & Manabe, S. Response of a coupled ocean-atmosphere model to increasing atmospheric carbon dioxide: sensitivity to the rate of increase. *J. Clim.* **12,** 2224–2237 (1999).
27. Watterson, I. G. Interpretation of simulated global warming using a simple model. *J. Clim.* **13,** 202–215 (2000).
28. Senior, C. A. & Mitchell, J. F. B. The time-dependence of climate sensitivity. *Geophys. Res. Lett.* **27,** 2685–2689 (2000).
29. Stainforth, D. A. *et al.* Evaluating uncertainty in the climate response to changing levels of greenhouse gases. *Nature* (submitted).
30. Allen, M. R. & Stainforth, D. A. Towards objective probabilistic climate forecasting. *Nature* **419,** 228 (2002).

Supplementary Information accompanies the paper on **www.nature.com/nature**.

Acknowledgements We thank A. Thorpe and M. Allen for encouraging the development of this project. We also acknowledge many Hadley Centre colleagues for their advice on model parameters and their uncertainty ranges, and for comments on earlier versions of the manuscript. This work was supported by the UK Department of the Environment, Food and Rural Affairs. D.A.S. was funded by the NERC COAPEC thematic programme.

Competing interests statement The authors declare that they have no competing financial interests.

Correspondence and requests for materials should be addressed to J.M.M. (james.murphy@metoffice.com).

Gigantism and comparative life-history parameters of tyrannosaurid dinosaurs

Gregory M. Erickson[1,2], Peter J. Makovicky[3], Philip J. Currie[4], Mark A. Norell[2], Scott A. Yerby[5] & Christopher A. Brochu[6]

[1]*Department of Biological Science, Florida State University, Tallahassee, Florida 32306-1100, USA*
[2]*Division of Paleontology, American Museum of Natural History, Central Park West at 79th Street, New York, New York 10024-5192, USA*
[3]*Department of Geology, The Field Museum, 1400 S. Lake Shore Drive, Chicago, Illinois 60605, USA*
[4]*Royal Tyrrell Museum of Palaeontology, Drumheller, Alberta T0J 0Y0, Canada*
[5]*Department of Biomechanical Engineering, Stanford University, Stanford, California 94305, USA*
[6]*Department of Geoscience, University of Iowa, Iowa City, Iowa 52242, USA*

How evolutionary changes in body size are brought about by variance in developmental timing and/or growth rates (also known as heterochrony) is a topic of considerable interest in evolutionary biology[1]. In particular, extreme size change leading to gigantism occurred within the dinosaurs on multiple occasions[2]. Whether this change was brought about by accelerated growth, delayed maturity or a combination of both processes is unknown. A better understanding of relationships between non-avian dinosaur groups and the newfound capacity to reconstruct their growth curves make it possible to address these questions quantitatively[3]. Here we study growth patterns within the Tyrannosauridae, the best known group of large carnivorous dinosaurs, and determine the developmental means by which *Tyrannosaurus rex*, weighing 5,000 kg and more, grew to be one of the most enormous terrestrial carnivorous animals ever. *T. rex* had a maximal growth rate of 2.1 kg d^{-1}, reached skeletal maturity in two decades and lived for up to 28 years. *T. rex*'s great stature was primarily attained by accelerating growth rates beyond that of its closest relatives.

Stemming from more than a century of investigation, considerable understanding of tyrannosaurid osteology[4], myology[5], neurology[6], behaviour[7,8], physiology[3,9], physical capabilities[10,11] and phylogeny[12,13] have been gained. Lacking are empirical data on tyrannosaurid life history such as growth rates, longevity and somatic maturity (adult size) from which the developmental possibilities for how *T. rex* attained gigantism can be formally tested.

Recent advances in techniques for determining the ages at death of dinosaurs by using skeletal growth line counts[3,14], coupled with developmental size estimates[3], make quantitative growth-curve reconstructions for dinosaurs feasible. These methods have been used to study growth rates in two small theropods, a small and a large ornithischian and a medium-sized and a gigantic sauropodomorph[3]. These data were used to derive a regression of body mass against growth rate and to generalize broadly about non-avian